Stetsenko et al. Nanoscale Research Letters (2017) 12:348
DOI 10.1186/s11671-017-2107-8

Nanoscale Research Letters

NANO EXPRESS Open Access

Optical Properties of Gold Nanoparticle Assemblies on a Glass Surface

M. O. Stetsenko[1*], S. P. Rudenko[1], L. S. Maksimenko[1], B. K. Serdega[1], O. Pluchery[2] and S. V. Snegir[2,3]

Abstract

The assemblies of cross-linked gold nanoparticles (AuNP) attract lot of scientific attention due to feasible perspectives of their use for development of scaled contact electrodes. Here, we developed and tested method of solid-state formation of dimers created from small AuNP (~18 nm) cross-linked with 1.9-nonadithiol (NDT) molecules. The morphology of created coating of a glass surface and its optical-polarization properties have been studied in detail by combination of scanning electron microscopy, atomic force microscopy, UV-visible spectroscopy, and modulation-polarization spectroscopy.

The modification of localized surface plasmon resonance (LSPR) of single AuNP and their assemblies were studied by measuring of the spectral characteristics of polarization difference at all stages of synthesis. The radiative and nonradiative modes of LSPR have been analyzed in detail at different angles of incidence light. This allowed establishing relation between surface morphology of the coating and its optical properties.

Keywords: Gold nanoparticles, Dimers, Localized surface plasmon resonance, Coupling, Modulation-polarization spectroscopy

Background

Thin films of cross-linked gold nanoparticle (AuNP) have received considerable scientific attention during the past two decades. Two- and three-dimensional arrays of metallic nanoparticles allowed to create downscaled contact electrodes [1–5]; touch sensors [6, 7]; and optically [8–10], chemically [11], and mechanically controlled [12] resistors. The architecture of nanoparticle assemblies can be controlled by employing of AuNP with various size, shape [1, 13], and by modification of the interparticle spacing. This distance can be changed by selecting of appropriate cross-linking agent, for instance alkyldithiol- [2–4] or thiol-terminated molecules with specific functional properties [9, 10]. To achieve self-organization of AuNP, the DNA chains [1, 5] can be employed also.

A variation of the interparticle spacing allows to tune optical properties of entire material by controlling amplitude and position of a localized surface plasmon resonance (LSPR) of the cross-linked nanoparticles at nanoscale [7–9, 14]. Therefore, a lot of attention is paid for this issue. An understanding of relation between morphology and optical properties of AuNP assemblies can provide a fundamental basis for further development of the scaled nanoelectronic devices based on gold nanoparticles cross-linked with organic molecules with various functional properties.

However, developing and engineering of the corresponding nanostructures with reproducible architecture and preassigned optical properties is a subject of continuous efforts [15, 16]. A lot of attentions is paid to create AuNP assemblies with controllable architecture especially AuNP dimers, since they can be considered as the model of two gold nanoelectrodes linked by molecules with required functionality. Different pathways of dimer synthesis in liquid media were employed. Some of them proposes to control relative concentration of ethanol in water colloidal solution of AuNP [15, 17], while others to use various passivation agents [16, 18], multivalent thiol ligands [19, 20], and dithiol molecules [16, 21]. However, the further application of these AuNP assemblies in a molecular electronics becomes infeasible since it require integration into electronic circuits. Thus, two main

* Correspondence: stetsenkomax@gmail.com
[1]V.Lashkaryov Institute of Semiconductor Physics, National Academy of Sciences of Ukraine, 45, Av. Nauky, Kyiv 03028, Ukraine
Full list of author information is available at the end of the article

challenges exist. First is to develop suitable method of solid-state synthesis which would occur directly on a solid surface of a conductive electrode. The second one is to achieve required optical properties of an electrode covered by AuNP assemblies. Therefore, the AuNP surface density, orientation toward incident light, and interparticle distance should be controlled during synthesis. In this relation, the LSPR which is monitored by UV-visible optical spectroscopy is expected to scale with the amount of AuNP and interparticle distance. When AuNP dimers are deposited on a glass slide, the transmission spectrum exhibits two distinct extinction bands: one at a wavelength of the LSPR band of single AuNP used in the assembly and the other at a greatly red-shifted wavelength due to the plasmon coupling along the interparticle axis for AuNP dimers [22–24]. The first experimental observations of dependence of the plasmon oscillation modes from interparticle spacing of a dimer and its orientation [25, 26] toward the incident light polarization are found in a good agreement with the proposed theory [27].

Here, we report about effective and facile method of formation of AuNP dimers cross-linked with 1.9-nonadithiol (NDT) which occurs directly on a solid surface. The glass surface was chosen to model a surface of an indium tin oxide (ITO) with electrical conductivity properties. Moreover, we have used commercially available glass slides to assemble AuNP which were synthesized using Turkevich method. With this, we brought to light some experimental asperities of solid-state synthesis of dimers and difficulties of their identification. With scanning electron microscopy (SEM), atomic force microscopy (AFM), UV-visible spectroscopy, and modulation-polarization spectroscopy (MPS), we provided a practical guide about how to control functionalization of a glass surface with AuNP to create their assemblies and to study the optical properties of created material. The MPS is an effective optical technique for diagnostics and characterization of the LSPR modification at nanoscale within the films of noble metals and metal-dielectric nanocomposites [28–30]. We will show that the plasmonic effects are strongly dependent on surface morphology, i.e., dispersion of single nanoparticles on the surface, their aggregation, and dimers formation. The comparison of LSPR parameters and optical-polarization properties for corresponding nanostructures will be demonstrated in the features of the spectral characteristics of the polarization difference, $\rho(\lambda)$ and the angle of isotropic reflection $\theta_{\rho=0}(\lambda)$, which are measured by MPS technique.

Methods

Sample Preparation

Synthesis of AuNP occurred following the Turkevich method [31–33]. An aqueous solution of $HAuCl_4$ (2.5×10^{-4} mol.L^{-1}) was heated to the boiling point in an Erlenmeyer flask. Then 1 ml of an aqueous sodium citrate solution (1.7×10^{-4} mol.L^{-1}) was added with vigorous magnetic stirring. The obtained colloidal water solution of gold nanoparticles was stored at 4 °C in a refrigerator to avoid nanoparticle aggregation. The average size of AuNP was ~18 nm (Fig. 1a) as evidenced by transmission electron microscopy (TEM). AuNP have a round shape with distinguishable facets on their surface which is monitored by high-resolution transmission electron microscopy (h-TEM) (Fig. 1a, insert). Optical spectra of colloidal solution (Fig. 1b) exhibit the LSPR at a wavelength of 520 nm (Fig. 1b, red curve) which is responsible for ruby color of water colloidal solution of AuNP.

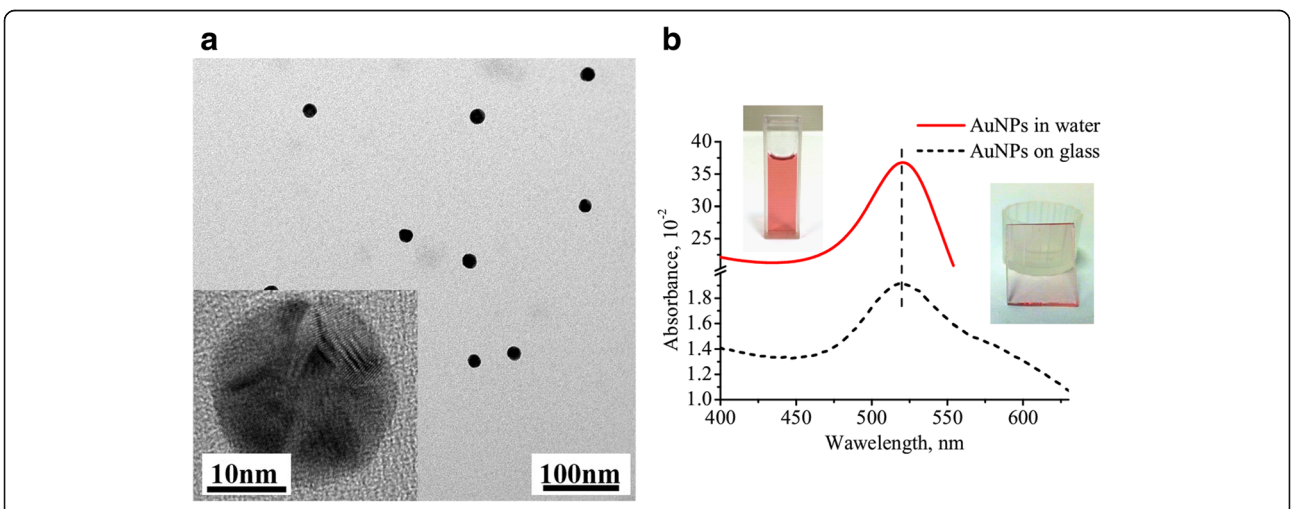

Fig. 1 TEM image of dried colloidal solution of AuNP (**a**).The *inset* on **a** is the image of single AnNPs obtained by h-TEM with *triangular-like dark/bright* regions revealing the presence of facets on the surface AuNP. The optical spectra (**b**) of AuNP colloidal solution (*red solid curve*) and of AuNP chemically attached to a glass surface (*black dashed curve*) by means of (3-aminopropyl)-triethoxysilane (APTES) monolayer

Glass slides (10×15 mm^2) were cut from commercially available cover slips (SCHOTT). The flatness of the surface was controlled by AFM, and the average roughness did not exceed 3 nm peak to peak. These slides were carefully cleaned several times in pure ethanol and dried in a flow of dry nitrogen. Finally, they were immersed in a methanol solution of (3-aminopropyl)-triethoxysilane (APTES) (0.21 mol $\times$ L^{-1}). After 3 h, the slides were sonicated in fresh methanol repeatedly (3×) to remove all physically adsorbed APTES molecules. The pre-coated glass slides (Fig. 2a, stage 1) with accessible NH_2 groups for AuNP anchoring were subsequently immersed by one side in an aqueous solution of the AuNP (the solution should keep its color during this process). The immersion occurred using polytetrafluoroethylene tweezers. The immersing time to form the first layer of AuNPs was equal to 20 min (sample name S20) and 30 min (S30). Variation of the time allowed to control the surface density of AuNP. The obtained slides covered by AuNP (Fig. 2, stage 2) were finally rinsed several times with pure water and dried in a flow of dry nitrogen.

Synthesis of AuNP dimers occurred on freshly coated with AuNP glass substrates (described above). The dried slides (S20, S30) were then immersed in ethanolic solutions of NDT ($c = 1.5 \times 10^{-3}$ mol.L^{-1}) for 30 s at ambient conditions to coat AuNP on a glass by dithiol molecule. In order to remove excessive physisorbed molecules, all substrates were rinsed successively in pure ethanol (HPLC-grade) and ultrapure water just after immersion in NDT without substrate drying. The position of initially deposited AuNP remained the same (see. Additional file 1: Figure S3). These wet substrates (S20, S30) were then immersed for the second time in a water colloidal solution of AuNP for 10 min (sample name S20/10) and 20 min (S30/20) correspondingly, with following rinsing with water and drying (stage 3). All chemicals were purchased from Sigma-Aldrich and used as received.

Methods

The AFM characterizations of AuNP attachment was performed by a Bruker Multimode apparatus operating in the PeakForce® mode and with apparatus manufactured by NT-MDT (Russia). All measurements were performed at ambient atmospheric conditions.

Optical spectra of the films were recorded using CARY 5000 spectrometer in transmission geometry at normal incidence within the wavelength range $\lambda = 400$–700 nm. SEM of glass surface covered by AuNP was performed using Zeiss Ultra55.

Spectral polarization characteristics for AuNP assemblies and AuNP dimers were measured in Kretschmann geometry using the modulation-polarization spectroscopy technique. The scheme of setup was described in detail in [34]. The MPS technique is based on modulation of polarization state of electromagnetic radiation, when the orthogonal components of linearly polarized waves (perpendicular (*s*) and parallel (*p*)) polarizations are alternately transformed at a constant intensity, frequency, phase, and wave vector. A diffraction monochromator MDR-4 (with a halogen tube KGM-150 at the input and Franck-Ritter polarizer at the output) served as a source of spectral radiation within the wavelength range $\lambda = 400$–1000 nm. A photoelastic polarization modulator (PEPM) acted as a dynamic phase plate. Alternating phase incursion was caused by compression/expansion of the quartz plate. A quarter-wave mode was selected by a proper supplying voltage. As a result, linear polarization was transformed into alternating right-to-left circular polarization. A stationary quarter-wave phase plate (PP) was placed after the PEPM. By rotating PP around the optical axis, a position of PP was selected at which polarization azimuths of radiation after PP alternated between parallel and perpendicular positions relative to the incident plane (*p*- and *s*-polarization, respectively). The output radiation was directed at a photodetector PD (silicon photodiode). Reflected light was a measure of the difference of orthogonally polarized intensities, which was transformed by a

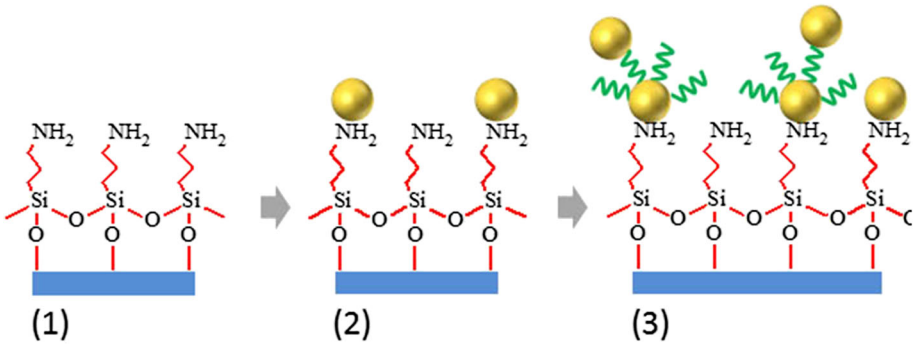

Fig. 2 Schema of stages of AuNP dimers formation on a glass surface. **1** Glass surface functionalized by APTES. **2** First immersion into water colloidal solution of AuNP. **3** Second immersion into fresh colloidal solution of AuNP occurred after functionalization of AuNP by NDT

PD into alternating signal. This signal was registered by a selective amplifier equipped with a phase-lock detector (lock-in-voltmeter) tuned to the modulation frequency of $f = 50$ kHz. The registered signal is the *polarization difference* $\rho(\lambda,\theta) = r_s^2 - r_p^2$, which is a magnitude of difference between the intensities of the internal reflection coefficients of *s*- and *p*-polarized light (r_s^2 and r_p^2, respectively). The parameter ρ is a Q component of the Stokes vector [35]. The refractive index of the quartz half-cylinder $n = 1.456$ determines the value of the critical angle of total internal reflection (TIR) as $\theta_{cr} = 43.6°$.

When the reflection coefficients of *s*- and *p*-polarized radiation have equal amplitude values, i.e. $r_s^2(\theta) = r_p^2(\theta)$, and the magnitude of polarization difference $\rho(\theta)$ equals zero, the light reflection occurs regardless of polarization state at the *angle of isotropic reflection* $\theta_{\rho=0}$ [36]. The condition of the isotropic reflection of electromagnetic radiation can be occured in the following cases: the first is a normal transmission/reflection of non-polarized radiation; the second is an attenuated internal reflection, when according to the Fresnel equations, the internal reflection coefficients of *s*- and *p*-polarized radiation are not equal at angles smaller than the critical angle ($r_s^2 < r_p^2$). The last case was realized in the present work. Each of these coefficients does not necessarily need to be zero. The equality of their magnitude is important.

Both ρ and $\theta_{\rho=0}$ parameters of MPS technique are mutually supportive and exhibit the features of spectral dependencies that caused by the optical-polarization properties of nanostructures with AuNP and characterize their resonant properties and features of surface morphology [29].

Results

Morphology and Optics Study

The AFM and SEM of S20 and S30 revealed that AuNP are randomly dispersed on a glass surface with some inclusion of aggregated nanoparticles (Additional file 1: Figure S1, S2). The coverage of the surface by single AuNP was calculated from AFM images and is equal to about 20/μm^2 and 60/μm^2 AuNP for sample S20 and S30, respectively. An analysis of the height profile (inset of Additional file 1: Figure S1b) of single AuNP confirms that they have an average diameter of ~18 nm. The color of the glass covered by AuNP becomes light pink (Fig. 1b, inset) due to LSPR of AuNP with $\lambda_{max} =$ 521 nm. The color of the slides did not change with the time as well as position of AuNP during AFM measurements revealing stability of AuNP coating.

Among single AuNP separated by a distance larger than one diameter (~18 nm), a few nanoparticles exhibit a coupling of their LSPR. This appears in the spectrum as shoulder in the long wavelength region at 550–650 nm (Fig. 1b). These nanoparticles are arranged in the objects without any distinct shape in which AuNP are separated from each other by a distance smaller than one diameter of AuNP (Additional file 1: Figures S1, S2). Therefore, such assemblies are responsible for the formation of broad light absorption band which is shifted to the longer wavelength region compared to LSPR of single AuNP. Noteworthy, these aggregates appear first after glass immersion into colloidal solution of AuNP giving stronger light absorption band after 20 min of immersion than LSPR of single AuNP (Fig. 3a). We suspect that at initial stage of AuNP assembling on a glass, they are attracted more intensively by some locale defects of the surface. Such aggregates were systematically present on the surface in spite of multiple cleaning of the glass slides after APTES adsorption. The nature of this effect requires additional attention and studies. However, with increasing of immersion time from 20 to 30 min, the ratio of single AuNP to their aggregates is progressively rising up. This leads to increasing of the LSPR band of single AuNP (Fig. 3a).

After functionalization of the AuNP surface with NDT molecules (Fig. 2), the position of LSPR adsorption band is changed due to modification of dielectric constant of

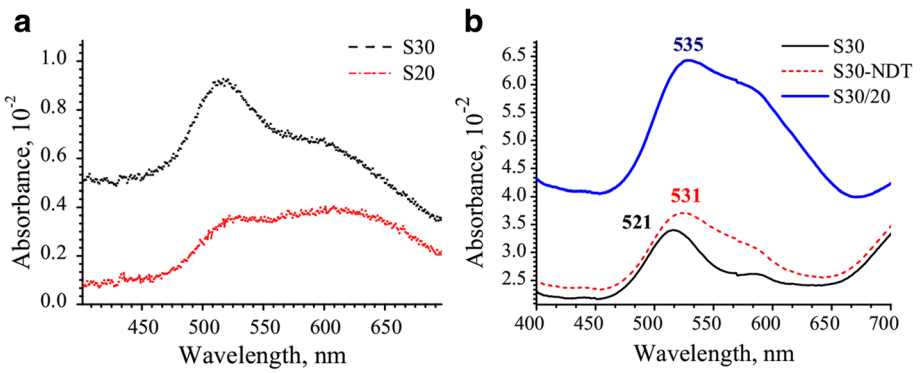

Fig. 3 Optical spectra for S20 (*bottom curve*), S30 (*top curve*) with characteristic LSPR band of single AuNP ($\lambda_{max} = 521$ nm) (**a**) and for S30 covered by NDT with following second immersion into AuNP solution to form dimers (S30/S20) (**b**)

AuNP surrounding media [37, 38]. The position of LSPR band of single AuNP consequently shifts to ~10 nm to longer wavelengths (Fig. 3b). Meantime, the position of λ_{max} for AuNP aggregates did not change.

The optical spectra of the glass surface with AuNP dimers (S30/20) revealed strong increase of overall intensity (Fig. 3b). The position of λ_{max} of LSPR of single AuNP is undergoing minor changes also. The small shift to longer wavelength is attributed to appearance of longitude optical excitation mode in AuNP dimers. Similar results were observed for AuNP colloidal solution with ~20% of AuNPs dimers linked by various dithiol molecules. However, simultaneously with the formation of dimers, the number of new single AuNP attached to a glass as well as AuNP linked to existed aggregates is growing also.

Thus, we performed AFM and SEM characterization of the sample S30/S20. The AFM measurements (Fig. 4a) allowed observing AuNP dimers, longitudinal axis of which is tilted to a plane of glass surface. Thus, the expected height of these dimers was in the range of 19.6–37.6 nm if considered that the length of NDT molecule and diameter of AuNP are equal to ~1.6 and 18 nm, correspondently. The quantity of such dimers, as seen from Fig. 4a, is very low. The closed-packed dimers and the ones with parallel axis to the surface were difficult to recognize due to limited resolution of AFM. This we overcame by the use of SEM (Fig. 4b). The red circles point to the positions of AuNP dimers. The measured spacing between the nanoparticles of the dimers is equal to ~20 nm. An analysis of SEM and AFM images revealed that the overall percentage of synthesized dimers is equal to about 11.6% (Table 1).

MPS Study

Optical-polarization properties and particularly plasmonic effects have been studied for the single AuNP in comparison with AuNP dimers using MPS technique by measuring the spectral characteristics of polarization difference $\rho(\lambda)$ in the different angular regions relatively to the angle of total internal reflection $\theta cr = 43.6°$ (Fig. 5). We have analyzed radiative (Fig. 5a) and non-radiative (Fig. 5b) modes of LSPR and paid attention to the dimers contribution in spectral characteristics $\rho(\lambda)$.

In Fig. 5a, the spectral characteristic of $\rho(\lambda)$ are shown in radiative region at the incident angle of $\theta = 35° < \theta cr$. All curves of $\rho(\lambda)$ have difference in amplitude and exhibit their minima with a peak position at a wavelength of 520, 544, 542, and 535 nm for sample S30, S20, S20/10, and S30/20, respectively. This difference we analyzed further with respect to the stage of glass surface functionalization (Fig. 2) and the time of immersion of glass slides in AuNP colloidal solution.

The shortest time of the first immersion of a glass into AuNP colloidal solution was equal to 20 min (Fig. 2) and led mainly to formation of the aggregates without any distinct internal packing structure. Consequently, we observed the LSPR at 544 nm (Fig. 5a, curve S20). With the longer immersion time (S30), the number of single AuNP grew up, as it clearly indicated by UV-visible spectra on Fig. 3a. Thus, MPS revealed shift of minima from 544 nm (S20) to 520 nm (S30) (Fig. 5a) since the Frohlich frequency for small AuNP gave stronger impact on formation of the band [39, 40]. Changing of packaging density of AuNP simultaneously with formation of AuNP dimers possessing a transverse plasmon coupling mode can lead to this spectral shift [22, 23]. Among shifting, the overall amplitude value of $\rho(\lambda)$ is increasing. Thus, the sample S30 demonstrates the highest reflection properties of single AuNP (Fig. 5a).

The correspondent growing of the amplitude values for samples S20/10 and S30/20 was also observed (Fig. 2), when second immersion occurred after covering of

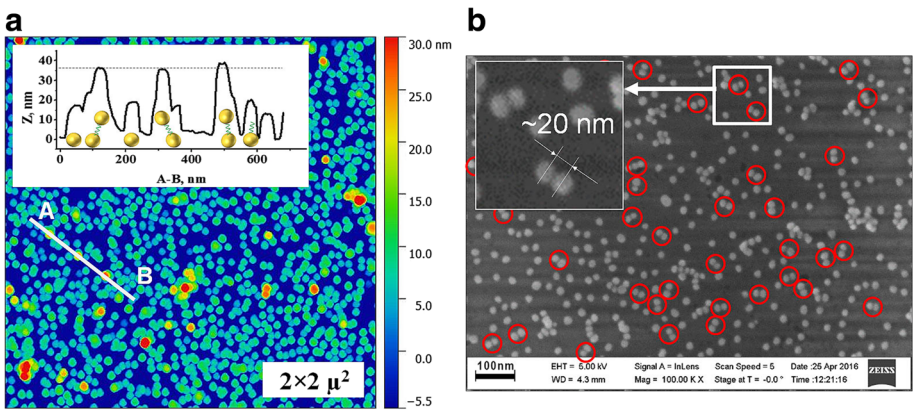

Fig. 4 AFM (**a**) and SEM (**b**) images of the sample S30/20. The *inset* on (**a**) is the cross section along *A-B* highlighting orientation of AuNP dimers according to measured height

Table 1 The quantity of AuNP objects calculated for sample S30/20 from SEM and AFM images

	Mono	Dimers	3*x*	4*x*	5*x*	*x* > 5	Total
Quantity	259	38	12	2	8	8	327
%	79	11.6	3.7	<1	2	2	100

AuNP with NDT. However, such growing has two origins. Simultaneously with increasing of the number of single AuNP which were attached by accessible amine groups, the formation of dimers and more complex objects was observed (Fig. 4). This, consequently, led to shifting of correspondent LSPR band for S30/20 compared to S30. Interesting, the minima for the sample S30/20 has much pronounced character than S20/10. We associate this with formation of dimers on S30/20 compare to S20/10. To understand the nature of formation of this minimum (Fig. 5a, blue curve), we have studied excitation features of the LSPR in nonradiative region at the incident angle of $\theta = 55°\theta > \theta cr$ (Fig. 5b). In the monitored wavelength region 450–1000 nm, each curve of $\rho(\lambda)$ is characterized by the presence of two extrema. The first one lies in the short wavelength range (450–550 nm) with positive values of amplitude $\rho(\lambda)$. It is attributed to the uncoupled dipole oscillations in single AuNP [41–43].

The second extremum is red-shifted with λ_{max} around 630 nm with negative value of amplitude of $\rho(\lambda)$. This extremum has two origins. It may appear as the result of the coupled dipole oscillation of longitude optical excitation mode along the dimer axis between the two nanoparticles [44]. At the same time, the dipole-dipole interactions within AuNP aggregates may give additional impact on extremum formation also [45]. Both of these types of coupling create the new collective oscillation modes. These modes are lower in energy than the surface plasmon of the individual AuNP. Therefore, it gives unique opportunity to distinguish clear difference between LSPR of single nanoparticle and that one with coupled LSPR.

Firstly, we consider the spectral features of $\rho(\lambda)$ for the functionalized glasses of AuNP with different immersion time (Fig. 5b). The reduction of AuNP quantity leads to small shift of extremum with negative values of amplitude of $\rho(\lambda)$ to longer wavelengths from 629 to 637 nm for samples S30 and S20, respectively. If we consider that at initial stage of AuNP attaching on a glass they form aggregates (Fig. 3a), the minima for S20 at 637 nm corresponds to closely packed AuNP without any internal structure. The lateral size of these aggregates is different which explains broadening of the spectrum contour appeared as the result of overlapping of LSPR [43]. With increasing of immersion time (S20→S30), the intensity of this band displays small growing. Simultaneously with this, we have observed small shift of λ_{max} from 637 to 629 nm. We do not have a clear explanation of this minor change so far but suspect that the process of aggregation which is caused by defects on a glass surface initially (S20) may have more complex nature with the longer immersion time.

With increasing of immersion time (S20→S30), the positive value of amplitude of $\rho(\lambda)$ at 502 nm undergo changes, as expected (Fig. 5b). This indicates that the number of single AuNP attached to the surface is growing. Initially for S20, as discussed above, only aggregates are formed on the surface. This is supported by the fact that amplitude of single AuNP at 502 nm for S20 (Fig. 5b) is much lower compare to S30.

With the formation of cross-linked AuNP using NDT alkyl dithiolthiol molecules, the intensities and what is more important shapes of all spectra (Fig. 5b) undergo changes. The shape of $\rho(\lambda)$ is typical for nanostructure with AuNP highly ordered arrays and is caused by the domination influence of linked AuNP. This linking leads to formation of more uniform oscillation band of AuNP for S20/10 compare to disordered aggregates of S20. For sample, S20/10 the λ_{max} of long wavelength extremum of $\rho(\lambda)$ is significantly shifted from 637 to 553 nm. This indicates about reduction of interparticle distance [39].

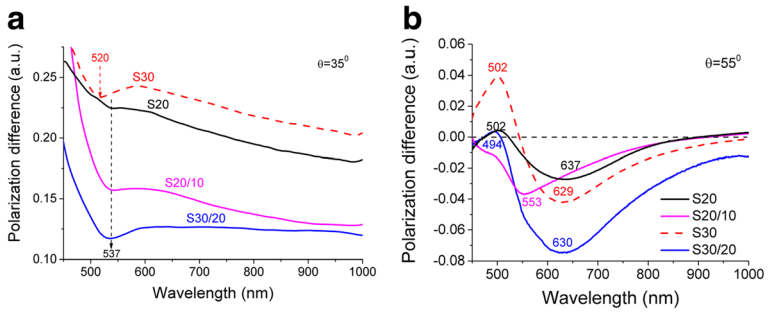

Fig. 5 Spectral dependencies of the polarization difference $\rho(\lambda)$ for samples S20, S30 of single AuNP, and S20/10, S30/20 of AuNP dimers at different incident angle of light: $\theta = 35°$ (**a**) and $\theta = 55°$ (**b**)

However, this shift cannot be attributed to significant increasing of density of single AuNP. This assumption is proved by minor changes of corresponding band at $\lambda_{max} = 502$ nm for S20/10 compare to S20. Therefore, we suspect that such progressive shift could be associated with the rearrangement of internal structure of AuNP aggregates when sample S20 was successively immersed into NDT and fresh AuNP colloidal solution. The formation of more uniformed structure of aggregates led to formation of more narrow absorption band (Fig. 5b) since the oscillation mode of cross-linked AuNP became similar (by energy) in all aggregates. We suggest following explanation of this effect. Initially, all aggregates have no distinct internal structure. As soon as aggregates became in contact with NDT solution, the surface of some AuNP in aggregates became partially modified by NDT molecules. Therefore, it is possible that due to minor mobility of these AuNP with NDT on a surface, they can become cross-linked. In addition, after the second immersion into fresh colloidal solution, these aggregates can bind even more AuNP. Consequently, the shell of aggregated object can contain AuNP separated on a distance equivalent to NDT length leading to formation of narrow light absorption band. Similar variation of the position of λ_{max} was observed in ref [46].

The behavior of the curve for sample S30/20 is different compare to S20/10. The position of the extremum of $\rho(\lambda)$ has minor changed. An additional small reflex at $\lambda_{max} = 553$ nm might be observed. This reveals about similar rearranging of the aggregated structure like for S20/10, as discussed above. However, the amplitude value of the curve for S30/20 is essentially increased. This is caused by growing numbers of cross-linked AuNP objects (Fig. 4) including 11.6% of dimers (Table 1). The broadening of the absorption band is remained the same. Obviously, it might be expected that dimers would give a single and more pronounced reflex in the spectra compared to disordered aggregated objects since longitudinal plasmon coupling mode is sensitive to the interparticle distance [24]. However, the correspondent band is not highly pronounced since the long axis of dimers has diverse orientation toward the incident light as it shown on Fig. 4. Moreover, the longer wavelength edge of $\rho(\lambda)$ above $\lambda > 700$ nm is possible associated with overlapping of plasmon's modes of oligomers and dimers [25, 26]. This range changed only for sample S30/20 whereas for sample S20/10, it remained the same as for S20 where formation of dimers was not expected. This observation is consistent with the fact that the sample S20/10 contains mainly AuNP aggregates which give the strongest impact on formation of correspondent spectra of $\rho(\lambda)$.

Discussion

A similar experimental studies of the spectral characteristic of polarization difference were performed for different incident angles θ that allowed to summarize the evolution of peak positions (Fig. 6a) and values of FWHM parameters (full width at a half maximum) (Fig. 6b) of LSPR for investigated samples. An increase of incident angle θ leads to long-wavelength shift of LSPR and increasing of FWHM. This is observed for sample S20 due to the presence of a large number of different AuNP aggregates on a glass surface. The peak position of LSPR for S20/10 is independent on the incident angle at the reduction of corresponding values of FWHM with increasing of incident angle θ. In this case, the surface electromagnetic wave does not develop, and its propagation is similar to a standing wave. This is typical for nanostructure with a large number of individual AuNP and AuNP aggregates that are not interact with each other's.

For the second type of sample S30/20 with dimers, the LSPR peak positions exhibit a weak dependency on the incident angle near a wavelength of ~ 626 nm. This result agrees with a studied of Hoon Cha and co-workers that was similarly observed a plasmon coupling in the AuNP dimers [44]. The values of FWHM parameters for dimer are increased, but on the other hand, with a weak

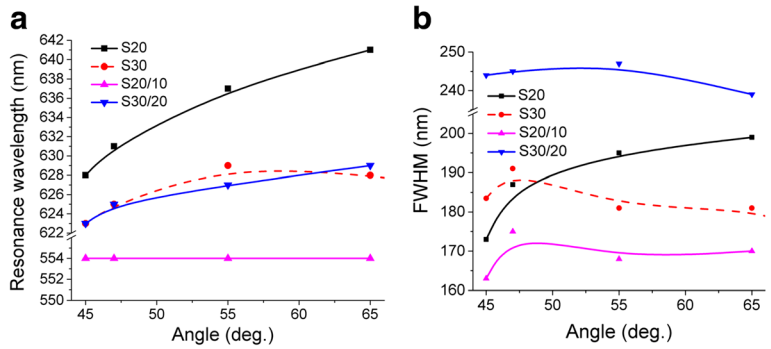

Fig. 6 Parameters of LSPR in dependence on the incident angle θ for samples S20, S30, S20/10, S30/20: **a** the peak positions of resonance and **b** values of FWHM parameters

dependency on the incident angle. It can be caused by the growing number of AuNP dimers and aggregates relatively to the single AuNP. Hence, among all investigated nanostructures, the optical-polarization features for sample S30/20 exhibited significant plasmon coupling, which shifted toward longer wavelength with increasing of the incident angle.

Note that the spectral characteristic of polarization difference includes the features of interaction between investigated nanostructures and simultaneously both parallel and orthogonal polarizations of electromagnetic radiation. They make a new contribution to the features of the spectra of $\rho(\lambda)$ for single AuNP and their dimers. Optical properties of single AuNP and their dimers also can depend on surface morphology and expressed direction of dimer axis relative to a glass surface [22, 23].

The size of nanoparticles and interparticle spacing can lead to existence of several mechanisms of the plasmon's interactions with electromagnetic waves on single non-interacting AuNP, their aggregates, dimers, and between them as a result of the dipole's field interactions between adjacent AuNP [47]. Dipole plasmons of individual NPs can hybridize to form the bonding dipole plasmon mode at lower energies, giving rise to enormous electromagnetic field enhancement at the nanogap, i.e., the "hot-spot" [48, 49]. For dimer's structure the role of gap size between nanoparticles an important and if this value is less than 2.8 nm the quantum size effect is influenced [50]. The plasmon coupling band for AuNP dimers shifts to blue wavelength region and becomes drastically broader due to disturbing of the plasmon coupling in the subnanometer regime by the electron tunneling effect [44, 51].

Thus, an investigation of resonant-optical properties of nanostructures with AuNP arrays depend on their sizes, shape and their mutual arrangement have been performed by measuring the spectral characteristics of the angle of isotropic reflection $\theta_{\rho=0}(\lambda)$ [29]. For nanostructures with single AuNP and AuNP dimers, the spectral characteristics of the angle of isotropic reflection $\theta_{\rho=0}(\lambda)$ are shown in Fig. 7 next to the appropriate spectral characteristics of polarization difference $\rho(\lambda)$ at the incident angle of $\theta = 43°$. All curves $\theta_{\rho=0}(\lambda)$ and $\rho(\lambda)$ exhibit the resonant character with extrema that coincide at appropriate wavelength positions. The extrema of $\theta_{\rho=0}(\lambda)$ resonances at $\lambda = 542$ and 560 nm for samples S20/10 and S30/20, respectively, for the AuNP dimers are blue shifted relatively to $\lambda = 600$ nm for both samples S20 and S30 of single AuNP. Moreover, these bands become broader with decreasing of interparticle distance of AuNP due to formation of AuNP dimers and increase of interaction between adjacent nanoparticles into AuNP aggregates. As a result of AFM measurements (Fig. 4a), the longitudinal axis of AuNP dimers is tilted to glass surface plane (Fig. 4). Obviously, the shape of dimers and aggregates that differs from spherical can be the reason for shifting of plasmon resonances. Similar shifting of

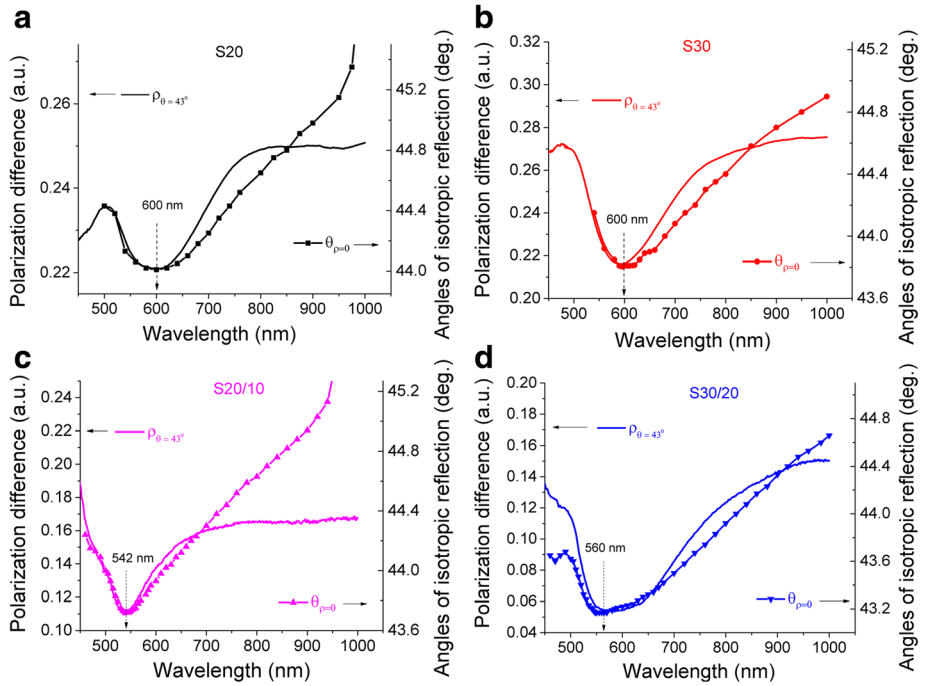

Fig. 7 Spectral dependencies of the angles of isotropic reflection $\theta_{\rho=0}(\lambda)$ in comparison with the spectral dependencies of the polarization difference $\rho(\lambda)$ at incident angle of light $\theta = 43°$ for samples S20 (**a**), S30 (**b**) of single AuNP, and S20/10 (**c**), S30/20 (**d**) of AuNP dimers

plasmon resonances in both red and blue wavelength directions in dependence on the changing of the nanoparticle shape was observed earlier [52].

In spite of the fact that the dipole-dipole interaction is attractive for *p*-polarization, which results in the reduction of the plasmon frequency (red shift of the plasmon band), while that for the *s*-polarization is repulsive, resulting in the increase in the plasmon frequency (blue shift) [41], the studying features of the isotropic reflection is unique because it reflects the change in the condition of equivalent interaction for both *s*- and *p*-polarization states of radiation that simultaneously interact with a nanostructure supported by MPS technique. It is known that natural oscillations of the conduction electrons or plasma oscillations of electrons in Au NPs are radiative modes. Correlation in extremum of the spectra of $\theta_{\rho=0}(\lambda)$ with the spectra of $\rho(\lambda)$ is observed in the vicinity to the critical angle of TIR θ_{cr} and in closeness to the radiative region ($\theta = 43° < \theta_{cr}$), which is caused by small mass thickness of all investigated samples and is generally associated with attenuated internal reflection of electromagnetic radiation. Apparently, the nature of the existing extrema of $\theta_{\rho=0}(\lambda)$ can be caused by average oscillations of plasmons in the AuNP due to generation of higher-order interactions between nanoparticles (quadrupole, etc.) when NP size increases and interaction transition mode from quasi-static to radiation is observed [53]. Moreover, even small intensity of exciting, electromagnetic wave can lead to strong oscillations, provided that the frequency of the incident radiation and the frequency of collective oscillations of conduction electrons in Au nanostructure are in resonance.

Conclusions

Thus, solid-state synthesis of AuNP dimers cross-linked with NDT molecules occurred directly on a glass surface coated by amine terminated molecules. These dimers have interparticle spacing determined by the length of NDT molecule. The orientation of the dimers on a glass surface is different. Major numbers of dimers are parallel to the surface of glass plane, while others have tilted orientation. This morphology of chemically attached dimers led to broadening of UV-visible absorption spectra and appearing of features in spectra of polarization difference $\rho(\lambda)$ under different angles of incident light. The growing number of AuNP dimers leads to broadening of LSPR band due to dominating influence of interparticle plasmon coupling that caused by decreasing of interparticle distance.

A detailed analysis of optical-polarization characteristics of LSPR in radiative and non-radiative wavelength regions allowed distinguishing between single AuNP, AuNP aggregates, and AuNP dimers in dependence on surface density of gold nanoparticles. A comparative study revealed that minor number of AuNP aggregates on a glass surface gave stronger optical absorbance compared to single AuNP. The initially disordered structure of these aggregates can undergo ordering when they are becoming in contact with NDT molecules in solution. This leads to formation of collective oscillation modes which are similar to AuNP dimers but oriented arbitrarily on the same surface. Therefore, study of the optical properties of AuNP dimers by MPS and UV-visible spectroscopy remains a complex task even when the complementary methods like AFM and SEM are used.

Additional File

Additional file 1: Figure S1. SEM images of AuNps chemically attached to glass surface for S30 (a) and AFM image of the same surface (b) with inset for cross-section along A-B. The image was obtained using commercially available AFM (Bruker, Germany) Immesion time of a glass in AuNP colloidal solution was 30 min. Figure S2. AFM images of the glass immersed into water colloidal solution of AuNP for 20 min (S20) and for 30 min (S30). Images were obtained using commercially available AFM (NT MDT, Russia). Figure S3. AFM image of the sample S30 after immersion into NDT. (DOC 790 kb)

Acknowledgements
SVS acknowledges the support of the Ministry of Education and Science of Ukraine and Ministry of Foreign Affairs of France (project DNIPRO 2015–2016, no. 34846NB).

Authors' Contributions
The manuscript was written through contributions of all authors. All authors have given approval to the final version of the manuscript.

Competing Interests
The authors declare that they have no competing interests.

Publisher's Note

Author details
[1]V.Lashkaryov Institute of Semiconductor Physics, National Academy of Sciences of Ukraine, 45, Av. Nauky, Kyiv 03028, Ukraine. [2]Institut des Nanosciences de Paris, Sorbonne Universités, UPMC Univ Paris-06, CNRS-UMR 7588, 4 place Jussieu, Paris, France. [3]Chuiko Institute of Surface Chemistry of National Academy of Sciences of Ukraine, Gen. Naumov str.17, Kyiv 03164, Ukraine.

Received: 31 December 2016 Accepted: 25 April 2017
Published online: 12 May 2017

References
1. Lu F et al (2015) Superlattices assembled through shape-induced directional binding. Nat Commun 6:6912
2. Rurack K (2012) Nanoparticle-based sensors: striped cation-trappers. Nat Mater 11(11):913–914
3. Bose SK et al (2015) Evolution of a designless nanoparticle network into reconfigurable Boolean logic. Nat Nanotechnol 10(12):1048–1052
4. Liao J et al (2015) Ordered nanoparticle arrays interconnected by molecular linkers: electronic and optoelectronic properties. Chem Soc Rev 44(4):999–1014
5. Ross MB, Ku JC, Vaccarezza VM, Schatz GC, Mirkin CA (2015) Nanoscale form dictates mesoscale function in plasmonic DNA–nanoparticle superlattices. Nat Nanotechnol 10(5):453–458
6. Segev-Bar M, Landman A, Nir-Shapira M, Shuster G, Haick H (2013) Tunable touch sensor and combined sensing platform: toward nanoparticle-based electronic skin. ACS Appl Mater Interfaces 5(12):5531–5541

7. Segev-Bar M, Haick H (2013) Flexible sensors based on nanoparticles. ACS Nano 7(10):8366–8378
8. Kim Y et al (2013) Stretchable nanoparticle conductors with self-organized conductive pathways. Nature 500(7460):59–63
9. Nishi H et al (2012) Plasmonic enhancement of gold nanoparticles on photocycloreversion reaction of diarylethene derivatives depending on particle size, distance from the particle surface, and irradiation wavelength. Phys Chem Chem Phys 14(14):4898
10. Fruhnert M et al (2015) Synthesis, separation, and hypermethod characterization of gold nanoparticle dimers connected by a rigid rod linker. J Phys Chem C 119(31):17809–17817
11. Ibañez FJ, Zamborini FP (2012) Chemiresistive sensing with chemically modified metal and alloy nanoparticles. Small 8(2):174–202
12. Olichwer N, Leib EW, Halfar AH, Petrov A, Vossmeyer T (2012) Cross-linked gold nanoparticles on polyethylene: resistive responses to tensile strain and vapors. ACS Appl Mater Interfaces 4(11):6151–6161
13. Borsley S, Flook S, Kay ER (2015) Binary nanoparticle planet–satellite assemblies †. Chem Commun 1:2–5
14. Lindquist NC, Nagpal P, Mcpeak KM, Norris DJ, Oh S (2012) Engineering metallic nanostructures for plasmonics and nanophotonics. Rep Prog Phys 75:036501 (61pp)
15. Tisserant J, Reissner PA, Beyer H, Fedoryshyn Y, and Stemmer A (2015) Water-mediated assembly of gold nanoparticles into aligned one-dimensional superstructures. Langmuir 31 (26), pp 7220–7227
16. Hussain I, Brust M, Barauskas J, Cooper AI (2009) Controlled step growth of molecularly linked gold nanoparticles : from metallic monomers to dimers to polymeric nanoparticle chains. Langmuir 8:1934–1939
17. Liao J, Zhang Y, Yu W, Xu L, Ge C, Liu J (2003) Linear aggregation of gold nanoparticles in ethanol. Colloids Surfaces A Physicochem Eng Asp 223: 177–183
18. Alivisatos AP (2010) Coupling of optical resonances in a compositionally asymmetric plasmonic nanoparticle dimer. Nano Lett 10:2655–2660
19. Song S, Kuang Y, Luo L, Sun X (2014) Asymmetric hetero-assembly of colloidal nanoparticles through "crash reaction" in a centrifugal field. Dalt Trans 1:5994–5997
20. Hofmann A, Schmiel P, Stein B, and Graf C (2011) Controlled formation of gold nanoparticle dimers using multivalent thiol ligands 27(24):15165-75.
21. Ranguwar NBR (2013) Discriminative response of aliphatic and aromatic dithiol in the self-assembly of gold nanoparticles. RSC Adv 3:15622–15625
22. Nordlander P, Oubre C, Prodan E, Li K, Stockman MI (2004) Plasmon hybridization in nanoparticle dimers. Nano Lett 4(5):899–903
23. Hao E, Schatz GC (2004) Electromagnetic fields around silver nanoparticles and dimers. J Chem Phys 120(1):357–366
24. Jung H, Cha H, Lee D, Yoon S (2015) Bridging the nanogap with light: continuous tuning of plasmon coupling between gold nanoparticles. ACS Nano 9(12):12292–12300
25. Brandl DW, Mirin NA, Nordlander P (2006) Plasmon modes of nanosphere trimers and quadrumers. J Phys Chem B 110(25):12302–12310
26. Chuntonov L, Haran G (2011) Trimeric plasmonic molecules: the role of symmetry. Nano Lett 11(6):2440–2445
27. Djuris AB (2013) UV–VIS and photoluminescence spectroscopy for nanomaterials characterization
28. Matyash IE, Serdega BK, Rudenko SP, Maksimenko LS (2011) Plasmonic optical properties and the polarization modulation technique. In: Mishchenko M (ed) Polarimetric detection, characterization, and remote sensing., pp 473–500
29. Stetsenko MO, Maksimenko LS, Rudenko SP, Krishchenko IM, Korchovyi AA, Kryvyi SB, Kaganovich EB, and Serdega BK (2016) Surface Plasmon's Dispersion Properties of Porous Gold Films. Nanoscale Res. Lett 11:116. doi: 10.1186/s11671-016-1327-7.
30. Grynko D a et al (2012) Modulation polarimetry of the topological effect in gold-organic nanocomposite films. Phys Solid State 54(11):2301–2308
31. Kimling J, Maier M, Okenve B, Kotaidis V, Ballot H, Plech A (2006) Turkevich method for gold nanoparticle synthesis revisited. J Phys Chem B 110:15700–15707
32. Turkevich J, Enustun B (1963) Coagulation of colloidal gold. J Am Chem Soc 85(21):3317–3328
33. Hillier J, Turkevich J, Stevenson PC (1951) A study of the nucleation and growth processes in the synthesis of colloidal gold. Discuss Faraday Soc 11: 55–75
34. Berezhinsky LJ, Maksimenko LS, Matyash IE, Rudenko SP, Serdega BK (2008) Polarization modulation spectroscopy of surface plasmon resonance. Opt Spectrosc 105(2):257–264
35. Born M, Wolf E (1980) Principles of optics (sixth edition): electromagnetic theory of propagation, interference and diffraction of light
36. Rudenko SP, Maksimenko LS, Matyash IE, and Mischuk OM (2016) Diagnostic of surface plasmons resonances in nanosized gold films by modulation polarization spectroscopy. Plasmonics 11(2):557–563
37. Bossard-Giannesini L, Cruguel H, Lacaze E, Pluchery O (2016) Plasmonic properties of gold nanoparticles on silicon substrates: understanding Fano-like spectra observed in reflection. Appl Phys Lett 109(11):111901
38. Snegir S, Mukha I, Sysoiev D, Lacaze E, Huhn T, Pluchery O (2016) Optically controlled properties of nanoparticles stabilised by photochromic difurylethene-base diarylethenes. Materwiss Werksttech 47(2–3):229–236
39. Maier S (2007) Plasmonics: fundamentals and applications. Springer, UK
40. Strizhevskii L, Dmitruk NL, Litovchenko VG (1989) Surface polaritons in semiconductors and insulators. Naukova Dumka, Kyiv
41. Jain PK, Huang W, El-Sayed MA (2007) On the universal scaling behavior of the distance decay of plasmon coupling in metal nanoparticle pairs: a plasmon ruler equation. Nano Lett 7(7):2080–2088
42. Rudenko SP, Stetsenko MO, Krishchenko IM, Maksimenko LS, Kaganovich EB, Serdega BK (2016) Surface plasmons in porous gold films. Opt Spectrosc 120(4):540–545
43. Losurdo M et al (2010) Size dependence of the dielectric function of silicon-supported plasmonic gold nanoparticles. Phys Rev B 82:23–25
44. Cha H, Yoon JH, Yoon S (2014) Probing quantum plasmon coupling using gold nanoparticle dimers with tunable interparticle distances down to the subnanometer range. ACS Nano 8(8):8554–8563
45. Diaz-Egea C, Abargues R, Martínez-Pastor JP, Sigle W, van Aken PA, Molina SI (2015) High spatial resolution mapping of individual and collective localized surface plasmon resonance modes of silver nanoparticle aggregates: correlation to optical measurements. Nanoscale Res Lett 10(1):310
46. Waldeisen JR, Wang T, Ross BM, Lee LP (2011) Disassembly of a core–satellite nanoassembled substrate for colorimetric biomolecular detection. ACS Nano 5(7):5383–5389
47. Song J-H KY-Y, Hong S-Y, Kim Y-G, Lee K-W (2007) Observation of plasmon hybridization in gold nanoparticle pairs. J Korean Phys Soc 50(3):558–562
48. Ma L, Zhang Z, Huang Y, Zhou Q, Hou M (2015) Nanogap effects on near- and far-field plasmonic behaviors of metallic nanoparticle dimers. Phys. Chem. Chem. Phys 7, 29293-29298
49. Huang Y, Ma L, Hou M, Li J, Xie Z, Zhang Z (2016) Hybridized plasmon modes and near-field enhancement of metallic nanoparticle-dimer on a mirror. Sci Rep 6:1–9
50. L Yang, H Wang, Y Fang, Z Li (2016) Polarization State of Light Scattered from Quantum Plasmonic Dimer Antennas. ACS Nano 10(1):1580–1588
51. Zuloaga J, Prodan E, Nordlander P (2009) Quantum description of the plasmon resonances of a nanoparticle dimer. NANO Lett 9(2):887–891
52. Gupta G et al (2009) Absorption spectroscopy of gold nanoisland films : optical and structural characterization. Nanotechnology 20:025703 (9pp)
53. Khlebtsov NG (2008) Optics and biophotonics of nanoparticles with a plasmon resonance. Quantum Electron 38(6):504–529